Research on Topological Grinding of Circumferentially Arranged Fish Scale Structured Surfaces on Inner Cylindrical Surfaces

Yuanzhi Qi, Xingshan Li* and Yushan Lyu

School of Mechanical Engineering, Shenyang Ligong University,
Shenyang, Liaoning, 110159, China
*Corresponding author's e-mail: lxs7241@sina.com

Abstract. Due to the excellent drag-reducing performance of fish scale surfaces in fluid environments, this study aims to grind a circumferentially arranged fish scale-structured surface on the inner cylindrical surface of a workpiece. Based on the characteristics of traveling wave structures and scale morphology, a fish scale surface model with circumferential arrangement on the inner cylinder was established, a topological mapping matrix was constructed, and a structured grinding wheel was designed. The effects of different speed ratios and grinding depths on the surface morphology were also investigated. The simulation results indicate that the designed grinding wheel can process a circumferentially ordered fish scale microstructure, and the grinding parameters have a significant regulatory effect on the texture morphology.

Keywords: inner cylindrical grinding; fish scale surfaces; structured grinding wheel; abrasive clusters

1 Introduction

In recent years, fish scale surfaces with traveling wave characteristics have garnered significant attention [1-2] due to their excellent drag-reducing performance in fluid environments. The key to achieving this drag reduction effect lies in the successful fabrication of surfaces with similar structural characteristics. Scholars both domestically and internationally [3-9] have proposed a series of innovative manufacturing techniques. For example, Piotr S. [3] used a diamond dresser to create millimeter-scale structured surfaces on conventional ceramic grinding wheels; Guo et al. [4] applied laser processing technology to produce structured grinding wheels for the surface machining of hard and brittle material workpieces. However, there is limited research on the grinding of inner cylindrical surfaces in the existing grinding studies, and the methods for designing grinding wheels based on workpiece surface morphological characteristics are also scarce.

In this study, a grinding wheel and grinding process suitable for the fish scale structured inner cylindrical surface were designed using a reverse solving method. The feasibility of the design was verified through simulation experiments, which also revealed the impact of grinding parameters on the texture characteristics of the inner fish scale surface.

2 Fish Scale Surface Characteristic and Model Establishment

2.1 Fish scale Unit Contour and Traveling Wave Structural Characteristics

Studies have shown that the surfaces of different types of fish scales [10] have common characteristics: overlapping scales, longitudinal staggered arrangement, and each scale consisting of four elliptical arcs (see Figure 1). Additionally, Figure 2 illustrates a schematic of the traveling wave indentations formed on a solid surface when in contact with fluid. The fish scale surface can be considered as a special type of traveling wave structured surface.

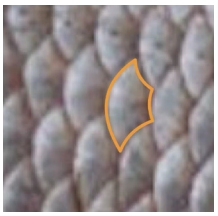

Fig. 1. Surface structure of fish scales.

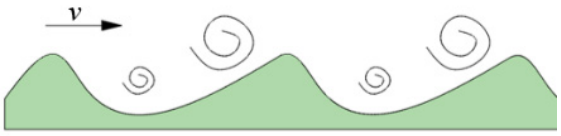

Fig. 2. Schematic diagram of the traveling wave structure.

2.2 The Model Establishment of the Inner Circular Fish-Scale Surface

Based on the contour analysis of the fish scale units, the schematic diagram of the inner cylindrical fish scale surface shown in Figure 3 was designed. The length l_w, width w_w, and depth d_w of the fish scale units are evenly divided. The length direction of the fish scale unit is divided into a equal units, and the width direction is divided into b equal units. By determining the position coordinates of the fish scale unit, the coordinate function in the depth direction can be obtained: $d_w = f_w(l_w, w_w)$. Therefore, the feature sets in the length, width, and depth directions of the fish scale units are:

$$\boldsymbol{L_w}=\begin{bmatrix} l_{w1} & l_{w2} & \cdots & l_{w(a-1)} & l_{wa} \end{bmatrix}^T,\quad \boldsymbol{W_w}=\begin{bmatrix} w_{w1} & w_{w2} & \cdots & w_{w(b-1)} & w_{wb} \end{bmatrix}^T$$

$$\boldsymbol{D_w}=\begin{bmatrix} d_{w11} & d_{w12} & \cdots & d_{w1(a-1)} & d_{w1a} \\ d_{w21} & d_{w22} & \cdots & d_{w2(a-1)} & d_{w2a} \\ \vdots & \vdots & \ddots & \vdots & \vdots \\ d_{w(b-1)1} & d_{w(b-1)2} & \cdots & d_{w(b-1)(a-1)} & d_{w(b-1)a} \\ d_{wb1} & d_{wb2} & \cdots & d_{wb(a-1)} & d_{wba} \end{bmatrix} \tag{1}$$

Thus, the topological feature vector $\boldsymbol{M_w}$ of the fish-scale unit can be expressed as:

$$\boldsymbol{M_w}=\begin{bmatrix} \boldsymbol{L_w} & \boldsymbol{W_w} & \boldsymbol{D_w} & 1 \end{bmatrix}^T \tag{2}$$

Based on the arrangement properties of the inner cylindrical fish scale structured surface, it is known that it is primarily related to the arrangement period $\boldsymbol{T_{xw}}$ in the $\boldsymbol{X_f}$ direction, the phase shift $\boldsymbol{\varphi_w}$ when staggered, and the arrangement period $\boldsymbol{T_{yw}}$ in the $\boldsymbol{Y_f}$ direction. Therefore, the arrangement vector $\boldsymbol{T_{fw}}$ of the inner cylindrical fish scale units can be established:

$$\boldsymbol{T_{fw}}=\begin{bmatrix} \boldsymbol{T_{xw}} & \boldsymbol{T_{yw}} & \boldsymbol{\varphi_w} \end{bmatrix}^T \tag{3}$$

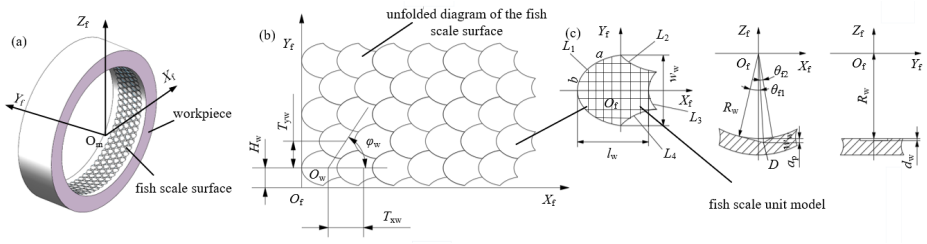

(a) Schematic diagram of the inner cylindrical surface of the workpiece (b) Unfolded diagram of the fish scale surface (c) Three-view diagram of the fish scale unit

Fig. 3. Schematic diagram of the arrangement of inner cylindrical fish scale units.

2.3 Structured Grinding Wheel Design

Based on the principles of inner cylindrical grinding and the topological mapping method, combined with the inner cylindrical fish scale structural unit model and its arrangement pattern, a schematic diagram of the grinding wheel fish scale abrasive cluster contour arranged circumferentially, as shown in Figure 4, was designed. The matrices for the unit length $\boldsymbol{L_s}$, unit width $\boldsymbol{W_s}$, and unit depth $\boldsymbol{D_s}$ of the abrasive cluster are as follows:

$$\boldsymbol{L_s}=\begin{bmatrix} l_{s1} & l_{s2} & \cdots & l_{s(a-1)} & l_{sa} \end{bmatrix}^T,\quad \boldsymbol{W_s}=\begin{bmatrix} w_{s1} & w_{s2} & \cdots & w_{s(b-1)} & w_{sb} \end{bmatrix}^T$$

$$\boldsymbol{D_s}=\begin{bmatrix} d_{s11} & d_{s12} & \cdots & d_{s1(a-1)} & d_{s1a} \\ d_{s21} & d_{s22} & \cdots & d_{s2(a-1)} & d_{s2a} \\ \vdots & \vdots & \ddots & \vdots & \vdots \\ d_{s(b-1)1} & d_{s(b-1)2} & \cdots & d_{s(b-1)(a-1)} & d_{s(b-1)a} \\ d_{sb1} & d_{sb2} & \cdots & d_{sb(a-1)} & d_{sba} \end{bmatrix} \tag{4}$$

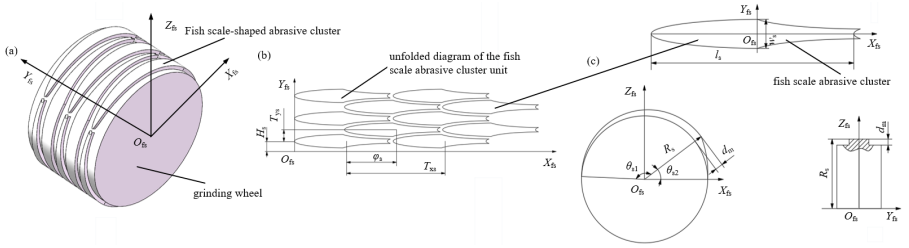

(a) Schematic diagram of the structured grinding wheel (b) Unfolded diagram of the grinding wheel surface (c) Three-view diagram of the abrasive cluster unit

Fig. 4. Schematic diagram of the fish scale structured grinding wheel.

Thus, the topological feature vector $\boldsymbol{M_s}$ of the grinding wheel abrasive cluster unit, the topological transformation matrix $\boldsymbol{T_{fs}}$ for the arrangement feature parameters of the grinding wheel abrasive cluster:

$$\boldsymbol{M_s}=\begin{bmatrix} \boldsymbol{L_s} & \boldsymbol{W_s} & \boldsymbol{D_s} & 1 \end{bmatrix}^T,\quad \boldsymbol{T_{fs}}=\begin{bmatrix} \boldsymbol{T_{xs}} & \boldsymbol{T_{ys}} & \boldsymbol{\varphi_s} \end{bmatrix}^T \tag{5}$$

The space occupied by the grinding wheel abrasive cluster unit can be regarded as a topological space $\boldsymbol{M_s}$, and the space occupied by the workpiece fish scale unit also constitutes a topological space $\boldsymbol{M_w}$. From a topological perspective, there exists a mapping relationship between them, namely: $\boldsymbol{M_w} \rightarrow \boldsymbol{M_s}$. Figure 5 shows a schematic diagram of grinding with a structured grinding wheel. In actual grinding motion, the grinding wheel only has feed motion in the circumferential direction, so the topological feature length $\boldsymbol{l_s}$ is stretched in the circumferential direction, while the width $\boldsymbol{w_s}$ remains unchanged. Based on the point set topology theory and grinding principles, the following topological mapping equations are established:

$$\boldsymbol{L_w}=\begin{bmatrix} \frac{\omega_s}{\omega_w} & \cdots & 0 \\ \vdots & \ddots & \vdots \\ 0 & \cdots & \frac{\omega_s}{\omega_w} \end{bmatrix}^{-1} \boldsymbol{L_s}+\begin{bmatrix} \frac{\tau\omega_s}{a\omega_w} & \cdots & 0 \\ \vdots & \ddots & \vdots \\ 0 & \cdots & -\frac{\tau\omega_s}{a\omega_w} \end{bmatrix}^{-1},\quad \boldsymbol{W_w}=\begin{bmatrix} 1 & \cdots & 0 \\ \vdots & \ddots & \vdots \\ 0 & \cdots & 1 \end{bmatrix}^{-1} \boldsymbol{W_s}$$

$$\boldsymbol{M}_w = \begin{bmatrix} \frac{\omega_s}{\omega_w} & 0 & 0 & -\tau\frac{\omega_s}{\omega_w} \\ 0 & 1 & 0 & 0 \\ 0 & 0 & -1 & 0 \\ 0 & 0 & 0 & 1 \end{bmatrix}^{-1} \boldsymbol{M}_s \quad \boldsymbol{T}_{fw} = \begin{bmatrix} \frac{\omega_s}{\omega_w} & 0 & 0 \\ 0 & 1 & 0 \\ 0 & 0 & \frac{\omega_s}{\omega_w} \end{bmatrix}^{-1} \boldsymbol{T}_{fs} \tag{6}$$

In these equations, $\boldsymbol{\omega}_S$ represents the angular velocity of the grinding wheel, and $\boldsymbol{\omega}_W$ represents the angular velocity of the workpiece.

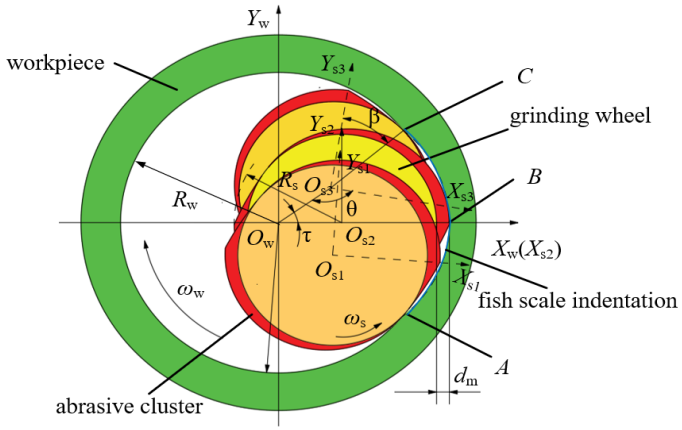

Fig. 5. Schematic diagram of grinding with a grinding wheel on the inner cylindrical surface.

3 Grinding Process Simulation Analysis

3.1 Simulation Conditions and Methods

According to the grinding motion principle shown in Figure 5, a structured grinding wheel model is first established using simulation software. By inputting grinding parameters, a motion simulation of the fish scale-structured surface is conducted to obtain the coordinates of the inner cylindrical surface of the workpiece. The model of the inner cylindrical surface is then evaluated to check for interference between the coordinate points and the surface. If interference is detected, the coordinate points are assigned to the nearest grid points, resulting in a complete fish scale-structured surface morphology. Due to potential deviations between the simulation results and the designed dimensions, let ξ represent the magnitude of the deviation, which is controlled within 1.25%.

$$\xi = \left| \frac{l_w}{w_w} - \frac{6.28}{5} \right| \times 100\% \tag{7}$$

A workpiece with an inner diameter of Φ40 mm, an outer diameter of Φ60 mm, and a width of 25 mm was selected. Each fish scale indentation unit was designed

with a unit length of 6.28 mm, a width of 5 mm, and a depth of 20 μm. Given the workpiece feed speed, for the stability of the grinding wheel during the grinding process and the aforementioned topological mapping relationship, the contour of the fish scale abrasive cluster unit was designed in the shape of an elliptical arc, with a major axis of 47 mm and a minor axis of 5 mm. The fish scale abrasive clusters are arranged in 2 units circumferentially and 5 rows axially. Given the workpiece feed speed $v_w = 3.14m/\min$, investigate the effects of different speed ratios ω_S/ω_-, i.e., p and grinding depths a_p on the surface morphology of the workpiece.

3.2 Effect of Grinding Depth on Workpiece Morphology

As shown in Figure 6, when maintaining a constant speed ratio of p=10 between the grinding wheel and the workpiece, a shallower grinding depth a_p (e.g.,10 μm) results in smaller indentation units, and gaps exist between these units, preventing overlap, thus displaying a separated state. As the grinding depth gradually increases, the size of the indentation units approaches the design specifications, and their arrangement changes, transitioning from a separated state to an adjacent state, and eventually, at greater grinding depths a_p (e.g.,30 μm), the units start to intersect or overlap.

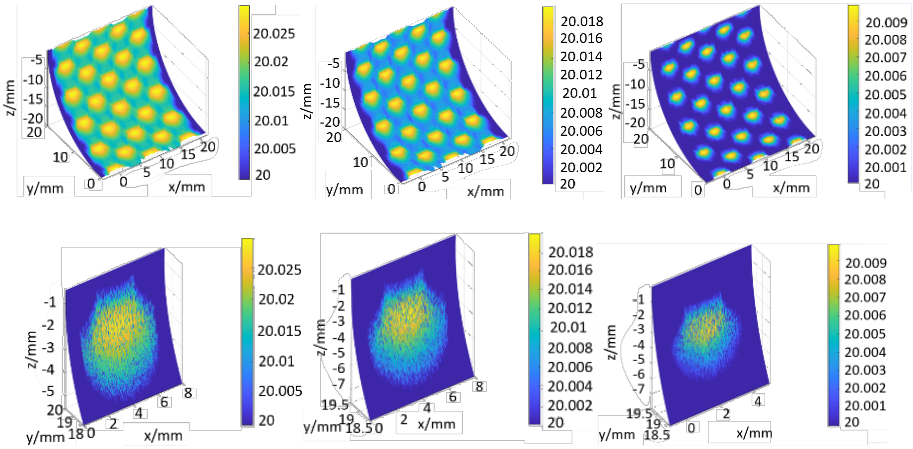

(a) v_w=3.14m/min, p=10, a_p=30μm; (b) v_w=3.14m/min, p=10, a_p=20μm; (c) v_w=3.14m/min, p=10, a_p=10μm.

Fig. 6. Simulation diagrams of the inner cylindrical surface of the workpiece ground at different depths of cut.

3.3 Effect of Speed Ratio on Workpiece Morphology

As shown in Figure 7, with the increase in speed ratio p, both the length of the fish scale units and their circumferential arrangement undergo significant changes. Specifically, when the p is relatively low (e.g.,5), the fish scale units are longer, and the

units are separated from each other, displaying a separated state. As the speed ratio p increases, the length of the fish scale units gradually shortens, transitioning from a separated state to an adjacent state (e.g.,10) and finally to an intersecting state (e.g.,15). A higher speed ratio leads to overlapping between the indentation units, reflecting an intersecting arrangement characteristic. Additionally, the number of fish scale units increases as the speed ratio increases, significantly enhancing the circumferential arrangement density. The characteristic values are shown in Table 1.

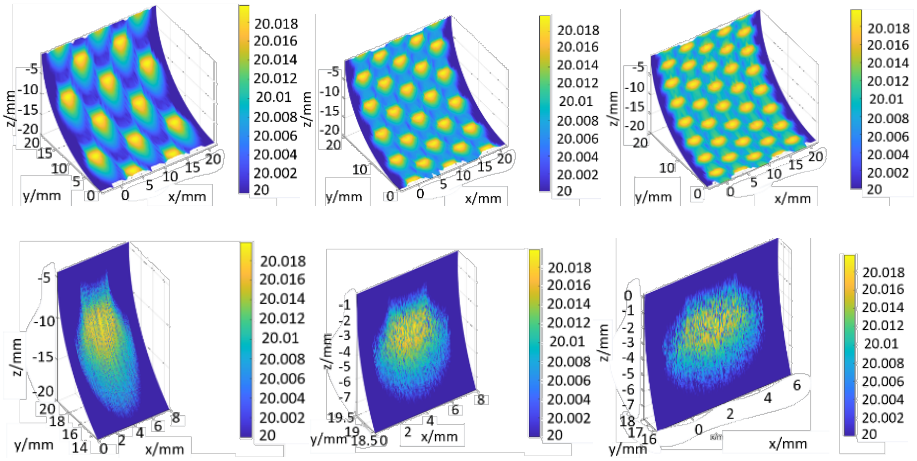

(a) v_w=3.14m/min, p=5, a_p=20μm; (b) v_w=3.14m/min, p=10, a_p=20μm; (c) v_w=3.14m/min, p=15, a_p=20μm.

Fig. 7. Simulation diagrams of the inner cylindrical surface of the workpiece ground at different spindle speeds.

Table 1. Comparison between the simulated pit parameters and the designed pit parameters.

Grinding Depth a_p /μm	Speed Ratio p	Length l_w/mm	Width w_w/mm	Depth d_w/mm	Deviation Value ξ
10	10	4.22	4.05	10	20.6%
20	5	12.44	5	20	123.2%
20	10	6.23	5	20	1.01%
20	15	4.07	5	20	44.2%
30	10	6.23	5	30	1.01%

4 Conclusion

By analyzing the contour of fish scale units and based on the principles of inner cylindrical grinding and point set topology theory, a circumferentially arranged fish scale-structured grinding wheel was designed and validated through simulation. The following conclusions were drawn: the topological mapping method enables

high-precision grinding of fish scale surfaces with errors controlled within 1.25%; different grinding parameters affect the morphology and arrangement of fish scale units (separated, adjacent, intersecting); due to the randomness of abrasive particle size, increasing abrasive density is necessary to ensure processing quality.

Acknowledgements

The authors gratefully acknowledge the support for this work from Chinese National Science Foundation (No.51875368)

Reference

1. Browning A, Ortiz C, Boyce C M. Mechanics of composite elasmoid fish scale assemblies and their bioinspired analogues [J]. Journal of the Mechanical Behavior of Biomedical Materials, 2013, 19 75-86. https://doi.org/10.1016/j.jmbbm.2012.11.003.
2. Wanting R, Haifeng Z, Tengjiao Z, et al. Drag Reduction Using Lubricant-Impregnated Anisotropic Slippery Surfaces Inspired by Bionic Fish Scale Surfaces Containing Micro-/Nanostructured Arrays [J]. Advanced Engineering Materials, 2020, 23 (1): https://doi.org/10.1002/adem.202000821.
3. Piotr S. Regular Surface Texture Generated by Special Grinding Process [J]. Journal of Manufacturing Science and Engineering, 2009, 131 (1): https://doi.org/10.1115/1.3070511.
4. Guo B, Zhao Q. On-machine dry electric discharge truing of diamond wheels for micro-structured sur-faces grinding [J]. International Journal of Machine Tools and Manufacture, 2015, 88 62-70. https://doi.org/10.1016/j.ijmachtools.2014.09.011.
5. Islam M M, Kim H, Han S D, et al. Convex diamond patterns by grinding with a wheel which is dressed by a rounded tool [J]. Journal of Mechanical Science and Technology, 2016, 30 (4): 1865-1873. https://doi.org/10.1007/s12206-016-0344-x.
6. Kim H, Ko J T. Verification of simulation of surface texturing on planar surface by grinding [J]. International Journal of Precision Engineering and Manufacturing, 2015, 16 (2): 225-231. https://doi.org/10.1007/s12541-015-0030-4.
7. Silva D J E, Bottene C A, Oliveira D G F J, et al. Grinding process for profiled texturing [J]. CIRP Annals - Manufacturing Technology, 2016, 65 (1): 337-340. https://doi.org/10.1016/j.cirp.2016.04.116.
8. Denkena B, Leon L, Wang B. Grinding of microstructured functional surfaces: a novel strategy for dressing of microprofiles [J]. Production Engineering, 2009, 3 (1): 41-48. https://doi.org/10.1007/s11740-008-0134-0.
9. Chen C, Tang J, Chen H, et al. An active manufacturing method of surface micro structure based on ordered grinding wheel and ultrasonic-assisted grinding [J]. The International Journal of Advanced Manufacturing Technology, 2018, 97 (5-8): 1627-1635. https://doi.org/10.1007/s00170-018-2044-4.
10. Muthuramalingam M, Puckert K D, Rist U, et al. Transition delay using biomimetic fish scale arrays. [J]. Scientific reports, 2020, 10 (1): 14534-14534. https://doi.org/10.1038/s41598-020-71434-8.